Advances in Intelligent Systems Research (AISR), volume 145
2017 International Conference on Electronic Industry and Automation (EIA 2017)

Micromachined Quartz Tuning Fork Gyroscope with High Overload Capacity

Maoyan FAN*
School of physics and Electronic Engineering
Yuxi Normal University
Yuxi, China
E-mail:fanmaoyan@vip.sina.com
+* Corresponding author

Lifang ZHANG
Office of Academic Affairs
Yuxi Normal University
Yuxi, China
E-mail:ff@yxnu.net

***Abstract*—To protect MEMS gyroscopes based on the quartz tuning fork in a high-g shock environment, the support bonding regions are located at where the stress concentrates in the spring beam of the tuning fork. After an analysis of the high overload shock characteristics, a highly efficient cushion structure is designed based on the ABAQUS finite element simulation. The cantilever-mass system is simplified to an equivalent mass attached to the end of the cantilever beam and the displacement response under the simple harmonic motion is simulated. A design of the position limit structure is explored and the strength distribution of the elastic quartz tuning fork is optimized. Therefore, the high shock resistance of 20,000g can be achieved and the good performance is maintained with an increase of the threshold by nearly 10 times.**

Keywords-high overload; quartz tuning fork; positions limit; cushion; reliability

I. INTRODUCTION

For the application of micromachined quartz tuning fork gyroscopes in the field of high overload dynamic testing, reliability is a hot research topic not thoroughly solved yet. This generally reflects in the bias drift after high overload and is embodied by the phenomenon that the zero-rate signal does not return to zero in the application. The existence of this error restricts its application fields so that the measurement data applied in a high overload environment cannot truly manifest the measured dynamic process and thus leading to difficulty in the data analysis and an ineffective measurement and control system [1,2]. The vibration and shock isolation technology used to improve the overload resistance of micromachined quartz tuning fork gyroscopes becomes an important research focus. The traditional theory of vibration and shock isolation is flawed and deficient for the dynamic analysis and design of strongly nonlinear systems with a big shock. M. A. Biot introduced the concept of shock response spectrum (SRS) in 1963 [3]. The equivalent damage principle is commonly used at home and abroad to simulate the complex shock oscillation environment. Optimization of structural design and taking measures of vibration and shock isolation enable cannon-launched guided projectiles to withstand the shock acceleration of 16000g at the moment of being projected by gyroscope and to be able to work normally after overload [4,5].

II. MICROMACHINED STRUCTURE AND WORKING PRINCIPLES

The micromachined quartz tuning fork gyroscope produces vibrations of an equal amplitude at the constant frequency under the action of the driving voltage and through the piezoelectric effect. The tuning fork in rotation is acted on by the Coriolis force to excite vibrations perpendicular to the original vibration plane, with an amplitude directly proportional to the rotational angular rate. The quartz tuning fork generates electric charges by the piezoelectric effect of vibration bending and senses the rotational angular rate. Its structure is shown in Fig.1.

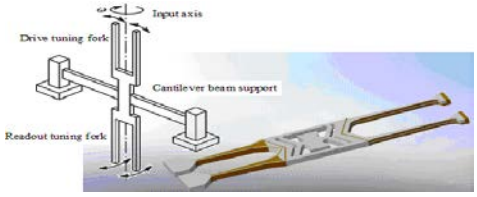

Figure 1. Micromachined quartz tuning fork

The quartz tuning fork gyroscope utilizes the structure of double tuning forks connected by an elastic cantilever beam. The upper drive tuning fork vibrates resonantly on the fork plane in the same direction or in opposite directions, and the lower sense tuning fork basically vibrates perpendicular to the fork plane under the Coriolis force, so as to counter the interference of the reference vibration to the angular speed signal. The vibration frequency of the sense tuning fork is close to that of the drive tuning fork, and the vibration amplitude of the sense tuning fork is directly proportional to the vibration amplitude and the input angular rate of the drive tuning fork. The electric charges generated by the piezoelectric effect of the sense tuning fork are converted by the charge amplifier circuit to be the voltage signals, which are amplified, filtered and demodulated to be DC voltage signals directly proportional to the input angular rate. Opposite vibration phases of the two tines of the sense tuning fork can neutralize the disturbing acceleration effect [6]. The micromachined tuning fork structure is sensitive to the angular rate only in one direction. The support and the cantilever beam are very important in the gyroscope microstructure. When the sense axis spins, the Coriolis force excites the sense vibration mode of the drive tuning fork, which is transferred to the sense vibration mode of the sense

tuning fork through the cantilever beam coupling. The bending coupling changed with time drives the sense mode by the frequency of the drive mode [7, 8].

III. Finite Element Analysis of Quartz Tuning Fork Gyroscope

The quartz tuning fork is considered as a kind of cantilever beam vibration among the bending vibrations. The design must have detailed information on the crystal size change, the electrical impact of support and other actual manufacturing requirements. First of all, the finite element analysis is used to calculate the resonant frequency, displacement, and stress distribution and obtain the characteristic curve of the design. The modeling process of the micromachined quartz tuning fork gyroscope is analyzing the quasi-static bending model under the sense mode. The bending cross section of a single tuning fork at the quasi-static sense mode under DC voltage is shown in Fig.2. The left side is the fixed end. The electrode is placed on the central axis Z_e and spreads the entire tine along the Y-direction. Its height in the Z-direction is h and the maximum displacement of the free end of the tine in the Z-direction is W_0.

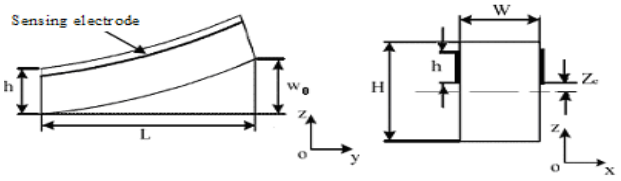

Figure 2. Bending and cross section of the sensing mode fork arm

The driving voltage generates an electric field along the X-direction and an axial stress along the Y-direction. The stress produces the bending moment. The displacement of the beam bending end is W_0. The axial stress in the Y-direction is polarized in the X-direction through the piezoelectric coefficient d_{12} of the quartz. The simplified model takes no account of the marginal effect of the electric field. The electric field ζ_x in the X-direction is V/W, the axial strain in the Y-direction is $\varepsilon_y = d_{12}\zeta_x$ and the corresponding Y axial stress is $\sigma_y = c_{22}d_{12}\zeta_x$, in which the stiffness constant equals to the value of c_{11}.

There are two factors for electrodes generating electric charges. (1) The dielectric polarization is caused by non-piezoelectric effects. The electric field ζ_x in the X-direction produces an electric displacement D_xE in the same direction, with an amplitude of $\varepsilon_{11}\zeta_x$ and the dielectric response of $hL\varepsilon_{11}\zeta_x$. (2) The piezoelectric response generates the electrode charges. The stress in the Y-direction produces a strain field D_xE in the X-direction, whose value is $d_{12}\sigma_y$, equal to $c_{11}d_{12}^2\zeta_x$. The electric charge of the piezoelectric response is $hLc_{11}d_{12}^2\zeta_x$. The following equation is obtained by combining these terms:

$$Q = Q_\varepsilon + Q_e \tag{1}$$

where:

$$Q_\varepsilon = \left[\varepsilon_{11}\left(\frac{hL}{W}\right)\right]V;\ Q_e = \left[c_{11}d_{12}^2\left(\frac{hL}{W}\right)\right]V \tag{2}$$

These two equations describe the relationship between electric charge and voltage of the quasi-static capacitance. Simplify the field marginal effect; we obtain the equivalent capacitance of the electrode:

$$C = C_0 + C_e \tag{3}$$

where:

$$C_0 = \left[\varepsilon_{11}\left(\frac{hL}{W}\right)\right]V;\ C_e = c_{11}d_{12}^2\left(\frac{hL}{W}\right) \tag{4}$$

A. *Parameters of the Sense Mode*

Resonant frequency under the sense mode:

$$\omega_{0,sense} = \sqrt{\left(5c_{11}H^2\right)/\left(6\rho_m L^4\right)} \tag{5}$$

$$f_{0,sense} = \omega_{0,sense}/2\pi \tag{6}$$

Coupling coefficient: $k_p = \sqrt{C_e/C_0} = d_{12}\sqrt{c_{11}/\varepsilon_0\varepsilon_{11}}$;
Dielectric capacitance: $C_0 = \varepsilon_0\varepsilon_{11}(hL/W)$;
Piezoelectric capacitance: $C_e = c_{11}d_{12}^2(hL/W)$;
Stiffness: $k = n^2/C_e$; Mass: $m = k/\omega_0^2$;
Damping: $b = m\omega_0/Q$; Resistance: $R = b/n^2$;
Inductance: $L = m/n^2$

B. *Parameters of the Drive Mode*

Resonant frequency under the drive mode:

$$\omega_{0,drive} = \sqrt{\left(5c_{11}W^2\right)/\left(6\rho_m L^4\right)} \tag{7}$$

$$f_{0,drive} = \omega_{0,drive} / 2\pi \tag{8}$$

Coupling coefficient: $k_p = \sqrt{C_e / C_0} = d_{12}\sqrt{c_{11} / \varepsilon_0 \varepsilon_{11}}$;
Piezoelectric capacitance:

$$C_0 = 8\varepsilon_0 \varepsilon_{11} L \sum_{l=1}^{odd} \frac{\cos(0.1l\pi)\left[\cosh(l\pi W / H) - 1\right]}{l\pi \sinh(l\pi W / H)} \tag{9}$$

Piezoelectric capacitance:

$$C_e = 8C_{11} d_{12}^2 L \sum_{l=1}^{odd} \frac{\cos(0.1l\pi)\left[\cosh(l\pi W / H) - 1\right]}{l\pi \sinh(l\pi W / H)} \tag{10}$$

Stiffness: $k = n^2 / C_e$; Mass: $m = k / \omega_0^2$;

Damping: $b = m\omega_0 / Q$;Resistance: $R = b / n^2$;

Inductance: $L = m / n^2$; $b = m\omega_0 / Q$;

ABAQUS is an internationally leading software suite for the finite element analysis with the good generality and a simple operation interface. In the simulation calculation process, after the structural and geometric parameters, material characteristics, load and boundary conditions are input, the simulation system can automatically select the appropriate load increment and the convergence criteria for the optimization algorithm. Then users can control the numerical solution of questions without defining any parameters. The parameter values are gradually adjusted in the analysis process and finally the accurate solution is obtained. The following functional simulations are completed in the ABAQUS system: (1) the simulation analysis of static stress and displacement, including nonlinearity and linearity; (2) the dynamic simulation analysis, inclusive of the modal analysis, steady-state and random response analysis, and transient response analysis; and (3) the analysis of nonlinear dynamic stress and displacement, viscoelasticity and viscoplasticity.

The crystals for the finite element analysis of micromachined quartz tuning fork gyroscopes utilize a cutting angle rotating $+2^\circ$ around X -axis on the Z -plane. Fig.3 shows a 2D geometric model of the fork arm. The electrode array must generate a reverse induction field at the two arms to excite the plane vibration. According to the finite element analysis, Table I shows the elastic constants and physical parameters used for the quartz during calculation.

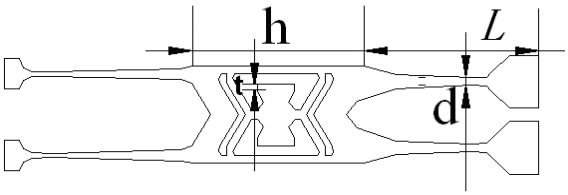

Figure 3. 2D geometric model of fork arm

($L = 3.5mm; d = 0.17mm$)

TABLE I. PHYSICAL PARAMETERS OF QUARTZ

Young's modulus	$E\left(c_{22}^{'}\right) = 8.9453\times10^{-10}$ (g · mm/s² · mm²)
Density	$\rho = 2.6487\times10^{-3}$ (g/mm³)
Poisson's ratio	$\delta\left(\frac{s_{12}^{'}}{s_{11}^{'}}\right) = 0.122894$

Definitions: base length denoted by (h); symmetric crystal: the arm has the equal length (L) and width (d); free vibration: the vibration F_f of crystal without support; clamping vibration: the vibration F_c after the crystal bottom is clamped, and the influence of bonding on the resonant frequency satisfies the following equation:

$$\Delta F_{cf} = \left(F_c - F_f\right) / F_c \tag{11}$$

In order to get the influence of the support, the simulation calculations have been conducted on the vibration frequency, displacement and stress distribution of free vibration and clamping vibration. The selected element type is C3D20 (hexahedral 20-node quadratic 3D solid element). The Static, General analysis steps are selected. The time step is set as 1, the initial increment size is set as 0.1, the minimum step size is $1e^{-5}$ and the maximum step size defaults as 1. Based on the finite element grid model and the load boundary conditions, the stress distribution when the driving end displacement is $10e^{-3}mm$ is shown in Fig.4. It can be seen from the simulation results that, as the driving end displacement increases, the maximum stress in the model increases linearly, and the convergence of two planes of the driving end has the maximum stress.

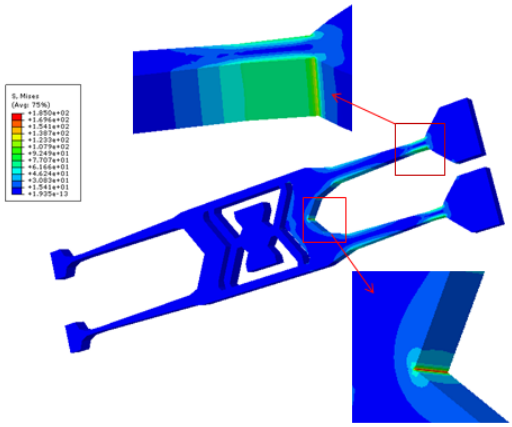

Figure 4. Stress distribution of the driving end displacement.

IV. STRUCTURAL OPTIMIZATION OF SHOCK-RESISTANT QUARTZ TUNING FORK

The micromachined quartz tuning fork gyroscope utilizes an integrated tuning fork structure and fabricated by the quartz MEMS techniques such as coating, photolithography, and etching. Due to the anisotropy of quartz tuning forks, the etch rate is different for each crystal orientation. At the tuning fork corner, it is etched to be the shape fit for the anisotropic characteristics of quartz crystal and not controlled by the shape of the etch mask. The stress concentrates at the corner profile. The stress concentration becomes more serious if the cross section size changes more radically, the angle is sharper and the aperture is smaller. As for the tuning fork structure made of brittle materials such as quartz crystal, under high overload, the maximum stress at the stress concentration positions first reaches the yield strength of the quartz crystal and the tuning fork structure breaks and damages. In order to improve the shock resistance of micromachined quartz tuning fork gyroscopes, the design must avoid the groove with a sharp angle structure or the small aperture. The arc transition is used at the corner. The structure with a big arc radius can ease the stress distribution here [9, 10].

A. *Influence of Bonding Position on the Vibration*

Table II shows the change of the base length (h) in Fig.3 and studies its influence on the fundamental frequency and vibration mode. Here, $h = 3.38mm$ represents the original model and the resonant frequencies correspond to $h = 3.38; 4; 4.5; 5mm$.

TABLE II. BASE LENGTH AND RESONANT FREQUENCY

h (mm)	6-order	7-order	8-order	9-order
3.38	9367.9	11060	13525	23297
4.0	10908	13341	14974	22972
4.5	12383	15102	16929	23657
5.0	13676	16947	18638	23725

B. *Influence of the Bonding Base Size*

The fundamental frequency corresponding to the change of t in Fig.3 is shown in Table III below, such as increment of 0.1mm or 0.2mm of the t height. It can be seen that the bonding base size has no obvious influence on the fundamental frequency and vibration mode.

The nodes of the free bar are usually used as the support points. Because these nodes are small points, the stress on them is big. However, the actual support points must have a certain area spreading to regions with large displacements, thus leading to the disturbance of the crystal vibration. The Q value is small and the temperature characteristic curve has considerable changes. Through analysis, it is found that the displacement and stress at the base of tuning fork crystal are small. That is to say, it can be used for bonding welding and has a very high shock resistance.

TABLE III. FUNDAMENTAL FREQUENCY OF THE BONDING BASE SIZE

Increment	6-order	7-order	8-order	9-order
0.1mm	9363.5	11056	13531	23275
0.2mm	9363.5	11057	13531	23278

C. *Modal Analysis of Quartz Tuning Fork*

The vibration mode is a very important design parameter for the micromachined quartz gyroscope under either forced vibration or sensitive vibration, both of which are in the state of resonant vibration. A finite element modal analysis is conducted on the micromachined quartz tuning fork gyroscopes. The boundary condition is all degrees of freedom restricted by the intermediate bonding positions. The selected analysis step is the Frequency and the 30-order vibration mode is solved. According to the working principles of the micromachined quartz tuning fork gyroscope, the seventh order is used as the drive mode and the eighth order is used as the sense mode. The tines of these two modes vibrate in different directions. The symmetric tuning fork structure can neutralize the acceleration disturbance. The simulation results are shown in Fig.5.

When changes of parameters affect the mode of the quartz gyroscope, the resonant frequency spacing of two vibrations is a major influencing factor of the bandwidth performance and sensitivity. The smaller the phase differences between them, the greater the sensitivity of the micromachined quartz tuning fork gyroscope. If they are too close, the bandwidth is small and the bias drift is large. Consideration of both is a basic principle for selecting the two resonant frequencies.

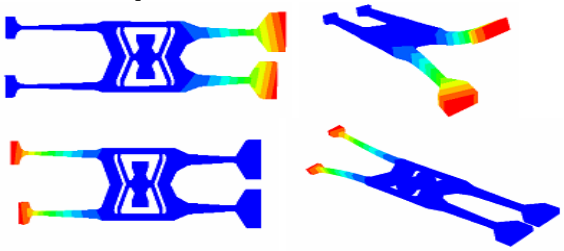

Figure 5. Quartz tuning fork modes of 7 and 8 order

D. *Analysis of the Anti-overload Stress*

The structural components of the micromachined quartz tuning fork gyroscope comprise tuning forks, proof mass, supporting beam and base. A high overload shock environment easily leads to adhesion and fracture, primarily the latter. The failure due to the Y -axis shock is more obvious than that due to the Z -axis shock. The shock resistance in the Z -axis direction is achieved by restricting the amplitude displacement and deploying cushion pads at the base, sealing cap and fork end. The cushioning performance of cushion pads is dependent on their cushioning efficiency. Under the same conditions, the larger energy they accumulate or absorb, the higher the cushioning efficiency. Therefore the shock isolation can be realized by using only a few cushion materials. The energy E

accumulated by the cushion material is the product of the material area A, the thickness h and the energy of the unit volume U_0.

$$E = h \cdot A \cdot U_0;\ U_0 = \int_0^{\varepsilon_m} \delta d\varepsilon \tag{12}$$

U_0 is the absorbed energy of the unit volume of cushion material, ε_m is the maximum strain, ε is the strain and δ is the stress. The experiment indicates that the special structure of porous foam aluminum has the nonlinear cushion characteristics [11, 12].

The boundary condition for the maximum stress analysis during rotation is restricting the motion of nodes on the rotation axis along the axis direction. The applied load is the rotational angular rate of 10000rad/s. The maximum stress already reaches 50MPa, close to two-thirds of the theoretical ultimate bending stress. As the rotation speed increases, the maximum stress of the tuning fork dramatically increases. The position with a maximum stress is at the convergence of two planes in the middle of the big end of tuning fork, where the stress concentrates. The centrifugal force is acted here by the tensile stress. The quartz is a kind of brittle material with poor tensile strength, so the transition should not be too sharp in the actual production process but utilize a smooth arc transition. Foam aluminum is a promising cushion material. The position limit design is used for the overload displacement response of the tuning forks. Considering the factors such as multipoint vibration reduction and contact area, it is calculated that the high shock resistance is 20,000g. The overload shock is far from the theoretical ultimate bending stress, so the quartz tuning fork will not break.

The bias voltage and threshold are measured after vacuum package of the quartz tuning forks. The measurement method is measuring noise when the gyroscope stably outputs after starting. The increment is $0.001^\circ / s$ per time. The output curve is recorded and the mean value is calculated. The signal-to-noise ratio of the output value reaches 63%. Then the input angular rate is the identifiable sensitivity limit called threshold. Fig.6 shows that the one-minute output curve when the input rate of micromachined quartz tuning fork gyroscope is $0.005^\circ / s$, thus it can be determined that the gyroscope threshold is $0.005^\circ / s$.

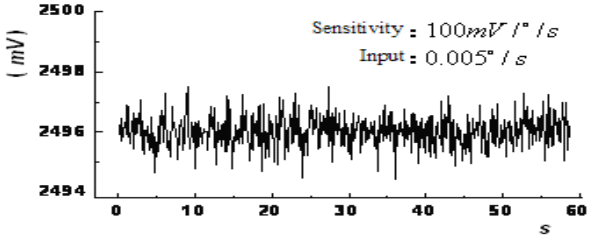

Figure 6. Micromachined quartz tuning fork gyroscope threshold.

V. CONCLUSION

The structural dynamic response of the micromachined quartz tuning fork gyroscopes under high overload is analyzed. The failure mode is the loosening of the bonding wire, rupture of the micro tuning fork, fracture of the fork ends, loosening of the fork and packaging base, and overall structural damage. The most vulnerable place is the flexible structure designed to improve the performance of the quartz tuning fork, which is prone to fracture and failure. Its structural parameters and processing quality are key factors that affect the reliability of gyroscopes. The high overload environment is easy to cause adhesion and fracture, primarily the latter. The failure due to the Y -axis shock is more obvious than that due to the Z -axis shock. It is difficult for the micromachined process to achieve position limit and vibration reduction. Optimization of the fork end and design of the arc structure of the fork combined with the end can enhance the overload resistance of the micromachined quartz tuning fork gyroscopes.

REFERENCES

[1] Yue Peng, Shi Zhen, Yang Ji, et al. GFMINS/GPS integrated navigation systems for high speed rocket projectiles[J]. J.Huazhong Univ. of Sci. & Tech. (Natural Science Edition), 2011, 39(11):10-14.

[2] C. Acar, A. R. Schofield, A. A. Trusov, L. E. Costlow, and A. M. Shkel. Environmentally robust MEMS vibratory gyroscope for automotive applications [J]. IEEE Sensors J. 2009, 9(12): 1895–1906.

[3] ZHANG Chunhui, WANG Yu, WU Yi hortg, et al. Shock response calculation and effects of structural parameters on shock isolation system with double displacement restrictors[J]. J0URNAL OF VIBRATION AND SH0CK, 2015, 34(5):12-130.

[4] WANG Shou-li, LIU Hai-tao, TENG Gang, LIU Er-jing, ZHANG Yu. Design method of MEMS IMU in high-g shock [J]. Journal of Chinese Inertial Technology [J]. 2014, 22(3):404-408.

[5] FAN Maoyan, TIAN Wenjie, ZHANG Lifang. Piezoelectric fluidic gyroscope with overload ability[J]. Journal of Yunnan University (NATURAL SCIENCE EDITION), 2004, 26(4A):85-88.

[6] Madni A M, Costlow L E, Knowles S J . Common design techniques for BEI Gyro Chip quartz rate sensors for both automotive and aerospace/ defense markets [J]. IEEE Sensor Journal, 2003, 3(5):569 - 578.

[7] Xuezhong Wu, Liqiang Xie, Jianchun Xing, et al.A Z-Axis Quartz Tuning Fork Micromachined Gyroscope Based on Shear Stress Detection[J].IEEE SENSORS JOURNAL, 2012,12(5):1246-1252.

[8] Hao Yanling, Liu Bo, Zhou Guangtao. Design of a MEMS gyroscope array with high sensitivity[J]. J. Huazhong University of Science & Technology (Natural Science Edition), 2014, 42(3):42-51.

[9] Wang Ying, Sun Yunan, Qin Bingkun. Study on the Modal Characteristic of Quartz Tuning-fork Angular Rate Micro-sensor by Means of FEM[J].SPIE, 2000,4222: 87-90.

[10] CUI Jiuzheng, SUN Bo, FENG Qiang. Finite Element Analysis of MEMS Package under High Impact [J]. JOURNAL OF MECHANICAL ENGINEERING, 2011, (47) 24: 177-185.

[11] LIU Jun, SHI Yunbo, MA Youchun. Experimental Analysis of Cushion Material in the Over Loading Test [J]. JOURNAL OF NORTH UNIVERSITY OF CHINA,2005, 5:381-384.

[12] Cheng Hefa, Huang Xiaomei, XU Ling. Investigation on compressive behavior and energy absorbing property of Al-Mg alloy foams[J]. Ordnance Material Science and Engineering, 2002, 25(6): 12-14.